Resource

SOURCE DATA | TRANSPARENT PROCESS | OPEN ACCESS | CHECK FOR UPDATES

THE EMBO JOURNAL

Conserved shifts in sperm small non-coding RNA profiles during mouse and human aging

Junchao Shi[1,2,11,13], Xudong Zhang[1,2,13], Chen Cai[1], Shichao Liu[1], Jiancheng Yu[3], Emma R James[1], Lihua Liu[1], Benjamin R Emery[1], Megan R McMurray Bires[1], Elizabeth Torres-Arce[1,12], Hukam C Rawal[4], Joemy Ramsay[1], Jason Kunisaki[3], Changcheng Zhou[2], David S Milstone[5], Mary Elizabeth Patti[6], Xiaoxu Yang[3], Tim G Jenkins[1,7], Aaron Quinlan[3], Bradley R Cairns[8], Paul Schimmel[9], James M Hotaling[1,10], Kenneth I Aston[1]✉, Tong Zhou[4]✉ & Qi Chen[1,2,3]✉

Abstract

Sperm aging impacts male fertility and offspring health, highlighting the need for reliable aging biomarkers to guide reproductive decisions. However, the molecular determinants of sperm fitness during aging remain ill-defined. Here, we profiled sperm small non-coding RNAs (sncRNAs) using PANDORA-seq, which overcomes RNA modification–induced detection bias to capture previously undetectable sncRNA species associated with mouse and human spermatozoa throughout the lifespan. We identified an "aging cliff" in mouse sperm RNA profiles—a sharp age-specific transition marked by significant shifts in genomic and mitochondrial tRNA-derived small RNAs (tsRNAs) and rRNA-derived small RNAs (rsRNAs). Notably, rsRNAs in mouse sperm heads exhibited a transformative length shift, with longer rsRNAs increasing and shorter ones decreasing with age, suggesting altered biogenesis or processing with age. Remarkably, this sperm head-specific shift in rsRNA length was consistently observed in two independent human aging cohorts. Moreover, transfecting a combination of tsRNAs and rsRNAs resembling the RNA species in aged sperm was able to induce transcriptomic changes in mouse embryonic stem cells, impacting metabolism and neurodegeneration pathways, mirroring the phenotypes observed in offspring fathered by aged sperm. These findings provide novel insights into longitudinal dynamics of sncRNAs during sperm aging, highlighting an rsRNA length shift conserved in mice and humans.

Keywords Sperm Epigenetics; Aging Clock; Sperm RNA Code; Paternal Age Effect; Epigenetic Inheritance
Subject Categories Methods & Resources; RNA Biology; Stem Cells & Regenerative Medicine
https://doi.org/10.1038/s44318-025-00687-8

Received 26 September 2025; Revised 4 December 2025; Accepted 12 December 2025
Published online: 20 January 2026

Introduction

In humans, fathers of advanced age are on the rise (Khandwala et al, 2017). Advanced paternal age not only compromises male fertility (Jimbo et al, 2022) but also poses risks to offspring health, associated with increased risks of stillbirth and a range of complications in subsequent generations, including elevated susceptibility to developmental, neuropsychiatric, and behavioral anomalies (Khandwala et al, 2018; Taylor et al, 2019). Beyond epidemiological evidence, rodent models have further reinforced the connection between paternal age and elevated risks of metabolic disorders, obesity, and anxiety-related behaviors (Guo et al, 2021; Mao et al, 2022). Traditionally, sperm aging research has focused on DNA integrity and methylation patterns (Ashapkin et al, 2023; Jenkins et al, 2014; Kunisaki et al, 2024; Neville et al, 2025; Seplyarskiy et al, 2025; Watson, 2025). However, recent discoveries have increasingly highlighted the epigenetic potential of mammalian sperm small non-coding RNAs (sncRNAs), including miRNAs, tRNA-derived small RNAs (tsRNAs), rRNA-derived small RNAs (rsRNAs), and their associated RNA modifications in mediating the intergenerational transmission of paternal environmental clues to offspring (Chen et al, 2016a; Chen et al, 2016b; Donkin et al, 2016; Gapp et al, 2014; Liu et al, 2023; Natt et al, 2019; Sarker et al, 2019; Sharma et al, 2016; Zhang et al, 2021; Zhang et al, 2018), including mediating age-related traits to the offspring (Guo et al, 2021; Liang et al, 2022; Miyahara et al, 2023). Sperm sncRNAs can also serve as biomarkers for embryo quality in IVF clinics (Hua et al, 2019;

[1]Molecular Medicine Program, Division of Urology, Department of Surgery, University of Utah School of Medicine, Salt Lake City, UT, USA. [2]Division of Biomedical Sciences, Center for RNA Biology and Medicine, School of Medicine, University of California, Riverside, CA, USA. [3]Department of Human Genetics, University of Utah School of Medicine, Salt Lake City, UT, USA. [4]Department of Physiology and Cell Biology, University of Nevada, Reno School of Medicine, Reno, NV, USA. [5]Department of Pathology, Brigham and Women's Hospital and Harvard Medical School, Boston, MA, USA. [6]Joslin Diabetes Center, Harvard Medical School, Boston, MA, USA. [7]Department of Cell Biology and Physiology, Brigham Young University, Provo, UT, USA. [8]Howard Hughes Medical Institute, Department of Oncological Sciences and Huntsman Cancer Institute, University of Utah School of Medicine, Salt Lake City, UT, USA. [9]Department of Molecular Medicine, The Scripps Research Institute, La Jolla, CA, USA. [10]Induction Bio, Salt Lake City, UT, USA. [11]Present address: China National Center for Bioinformation and Beijing Institute of Genomics, Chinese Academy of Sciences, Beijing, China. [12]Present address: School of Environmental and Life Sciences, The University of Newcastle, Callaghan, and Infertility and Reproductive Research Program, Hunter Medical Research Institute, New Lambton Heights, NSW, Australia. [13]These authors contributed equally: Junchao Shi, Xudong Zhang. ✉E-mail: ki.aston@hsc.utah.edu; tongz@med.unr.edu; qi.chen@hsc.utah.edu

Isacson et al, 2025). This has given rise to the concept of 'sperm RNA code' (Zhang et al, 2019), proposing that specific sperm RNA signatures, reflecting paternal experiences, play a critical role in controlling offspring health.

To decode the sperm RNA code, we developed PANDORA-seq (Shi et al, 2021), a novel method that overcomes limitations in traditional sncRNA sequencing by addressing RNA modifications (Shi et al, 2022), enabling comprehensive analysis of previously undetectable sncRNAs, particularly tsRNAs and rsRNAs with such modifications (Shi et al, 2021). PANDORA-seq has revolutionized our understanding of the sncRNA landscape in sperm, uncovering that miRNAs account for less than 1% of sperm sncRNAs, while tsRNAs and rsRNAs emerge as the dominant sperm sncRNAs that play critical roles in sperm-mediated epigenetic inheritance (Chen, 2022).

In this study, PANDORA-seq revealed a previously undetected 'aging cliff' in mouse sperm aging—a sharp transition in tsRNA and rsRNA profiles that traditional sncRNA-seq could not detect. Furthermore, analysis of sncRNAs in sperm heads uncovered an age-dependent length shift in rsRNAs, a phenomenon observed in both mice and humans. These findings suggest conserved mechanisms of sncRNA processing during aging, holding the potential for developing clinical biomarkers to assess human sperm aging and quality.

Results

PANDORA-seq reveals a sharp tsRNA/rsRNA "aging cliff" in mouse sperm

To analyze the sperm aging process in mice, we utilized the inbred strain C57BL/6J from Jackson Laboratory, organized into five age groups at 20-week intervals (10-, 30-, 50-, 70-, and 90-week old) (Fig. 1A). Mature sperm from the cauda epididymis (four mice per age group) were isolated for RNA extraction as previously described (Peng et al, 2012). The extracted sperm RNA from each individual was split into two portions: one for traditional sncRNA-seq and the other for PANDORA-seq. Sequencing data were annotated for different sncRNA types (e.g., miRNAs, tsRNAs, and rsRNAs) using the SPORTS tool (Shi et al, 2018) and further analyzed for age-related changes in sncRNA profile (see Methods). Through principal coordinate analysis (PCoA) of PANDORA-seq data (Fig. 1B), we observed a distinct 'aging cliff' between 50- and 70-week intervals, marked by a dramatic shift in tsRNA/rsRNA composition (computed across all tsRNA and rsRNA categories). This stark change delineated early (10–50 weeks) from late (70–90 weeks) stages, unlike traditional sncRNA-seq (Fig. 1B), which showed subtler changes, likely due to missed detection of highly modified sncRNAs.

In addition, we conducted a similar PCoA based on sperm miRNA composition by computing every miRNA expression. Intriguingly, even though miRNA reads constitute <0.5% of total reads in PANDORA-seq compared to >5% in traditional sncRNA-seq (Table EV1), the miRNA profile from PANDORA-seq still delineated an aging cliff between the 50- and 70-week intervals, which was not observed in traditional sncRNA-seq (Fig. EV1A–C). One possible explanation for this observation is that a subset of the miRNAs detected by PANDORA-seq are actually derived from tsRNAs and rsRNAs, a phenomenon we have previously reported (Shi et al, 2021). This result is somewhat unexpected given the low proportion of miRNA reads in the PANDORA-seq dataset, but it highlights the superior sensitivity of PANDORA-seq in detecting age-related changes within sncRNA populations, even when these changes are represented by a relatively minor fraction of the total reads. However, it should be noted that the 'aging cliff' identified by miRNAs between the 50- and 70-week intervals is less pronounced than that revealed by tsRNAs/rsRNAs. This difference is supported by the ratio of between-group variance to within-group variance (*F*-statistic) (Fig. EV1D), which is significantly higher for tsRNAs/rsRNAs compared with miRNAs, supporting a better separation between the demarcated stages (early 10-/30-/50-week vs. later 70-/90-week) using tsRNA/rsRNA profiles.

Since the primary part of sperm for fertilization is the information stored in sperm head, containing both the DNA and RNAs that are deeply embedded in the nuclei, these head-embedded RNAs are potentially more functionally relevant during the early epigenetic reprogramming events in the male pronucleus and in regulating embryo development (Chen, 2022). By contrast, RNAs present in the limited sperm cytoplasm are rapidly diluted in the oocytes at fertilization. Indeed, our previous study showed that the de-membranated sperm heads contain different sncRNA profiles compared to the intact sperm (Shi et al, 2021). Given the sperm head's unique sncRNA profile and function, we further performed PANDORA-seq and traditional sncRNA-seq on de-membranated mouse sperm heads across the same age groups as studied with whole sperm (10-, 30-, 50-, 70-, and 90-week-old). While there are differences in the sncRNA composition between sperm heads and whole sperm, both sample types revealed aging signatures indicative of an "aging cliff" at the 50–70 week transition for both tsRNA/rsRNA (Fig. 1C) and miRNAs (Fig. EV1E–H) using PANDORA-seq, a pattern not clearly observed with traditional sncRNA-seq. Individual tsRNA/rsRNA mappings for intact sperm (Fig. 1D) and heads (Fig. 1E) show substantial 50–70 week alterations, recapitulating the aggregate cliff by overall tsRNA/rsRNA profile.

Mitochondrial tsRNAs/rsRNAs in sperm heads parallel genomic sncRNA aging patterns

Interestingly, although the sperm head samples are completely depleted of sperm tail (Fig. 1F) and thus no mitochondria are included, we consistently detected mitochondrial tsRNAs (mt-tsRNAs) and mitochondrial rsRNAs (mt-rsRNAs) in the sperm heads. This resonates with the recent reports that mt-tsRNAs/mt-rsRNAs are sensitive to dietary stress (Cai and Chen, 2024; Natt et al, 2019; Ramesh et al, 2023) and act as signal molecules in controlling embryo development (Cai and Chen, 2024). We found that while the percentages of mitochondrial tsRNAs and rsRNAs are very low in the sperm head (0.14 and 0.11% respectively) (Fig. 1F), their levels are highly correlated, with coordinated up- or downregulation across age groups (Figs. 1G and EV2). Moreover, despite the low expression level of mitochondrial tsRNAs and rsRNAs compared to the genomic tsRNAs and rsRNAs, they effectively distinguish age groups, mirroring the genomic tsRNA/rsRNA aging cliff (Fig. 1H). This finding suggests that mitochondrial tsRNAs and rsRNAs, despite their low abundance, encode aging-relevant information that parallels genomic tsRNAs/rsRNAs.

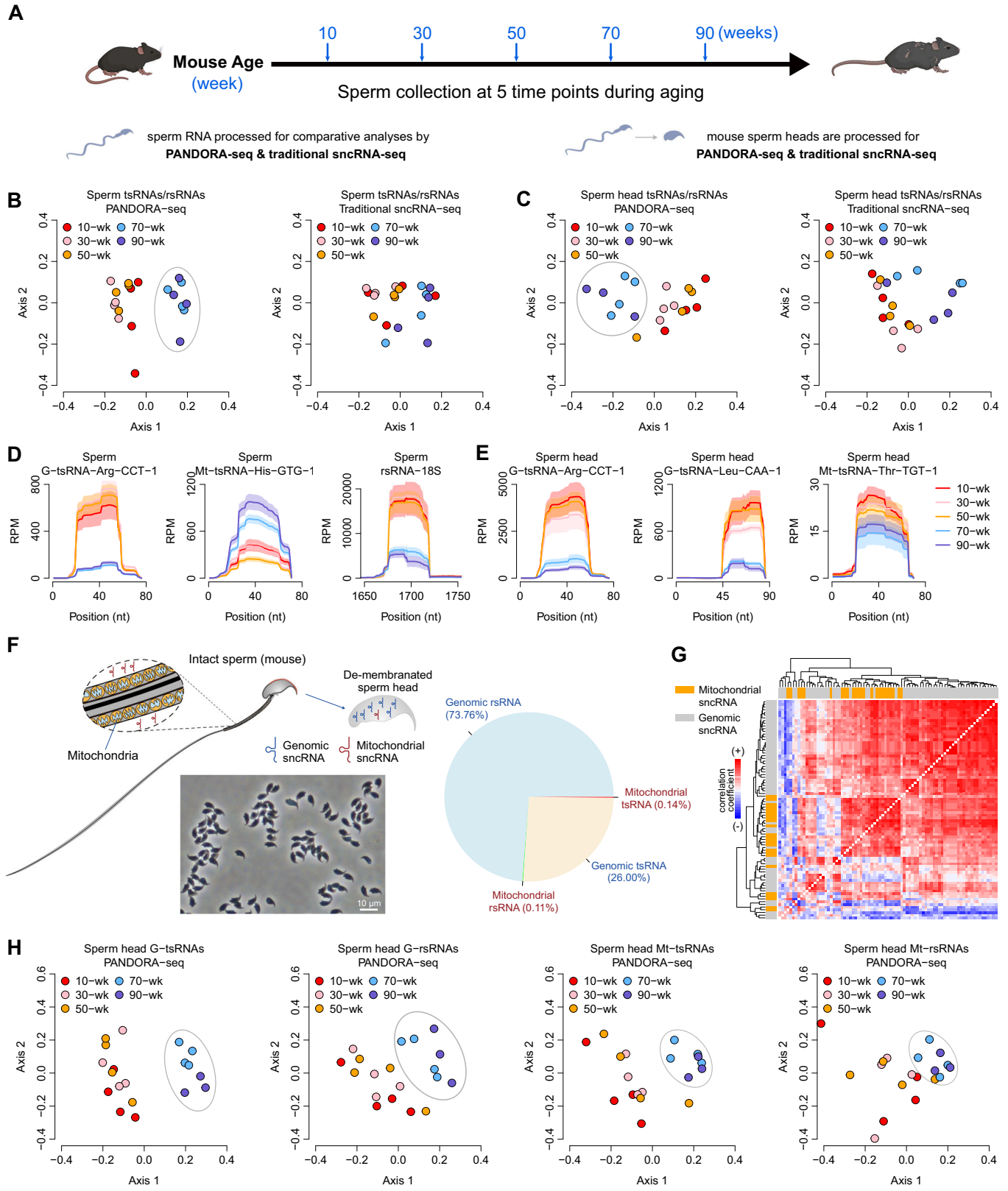
A
Mouse Age (week)
10
30
50
70
90 (weeks)
Sperm collection at 5 time points during aging
sperm RNA processed for comparative analyses by PANDORA-seq & traditional sncRNA-seq
mouse sperm heads are processed for PANDORA-seq & traditional sncRNA-seq
B
Sperm tsRNAs/rsRNAs PANDORA−seq
Sperm tsRNAs/rsRNAs Traditional sncRNA−seq
C
Sperm head tsRNAs/rsRNAs PANDORA−seq
Sperm head tsRNAs/rsRNAs Traditional sncRNA−seq
10−wk 30−wk 50−wk 70−wk 90−wk
Axis 1
Axis 2
D
Sperm G−tsRNA−Arg−CCT−1
Sperm Mt−tsRNA−His−GTG−1
Sperm rsRNA−18S
E
Sperm head G−tsRNA−Arg−CCT−1
Sperm head G−tsRNA−Leu−CAA−1
Sperm head Mt−tsRNA−Thr−TGT−1
RPM
Position (nt)
F
Intact sperm (mouse)
De-membranated sperm head
Mitochondria
Genomic sncRNA
Mitochondrial sncRNA
10 μm
Genomic rsRNA (73.76%)
Mitochondrial tsRNA (0.14%)
Genomic tsRNA (26.00%)
Mitochondrial rsRNA (0.11%)
G
Mitochondrial sncRNA
Genomic sncRNA
correlation coefficient
(+)
(-)
H
Sperm head G−tsRNAs PANDORA−seq
Sperm head G−rsRNAs PANDORA−seq
Sperm head Mt−tsRNAs PANDORA−seq
Sperm head Mt−rsRNAs PANDORA−seq

Figure 1. Discovery of an 'aging cliff' in mouse sperm sncRNA profiles using PANDORA-seq.

(**A**) Schematic of the experimental design: Sperm collected from C57BL/6J mice at 5 time points (10-, 30-, 50-, 70-, and 90-week; $n = 4$ per group) during aging, processed for comparative analyses by PANDORA-seq and traditional sncRNA-seq on intact sperm and de-membranated sperm heads. (**B**) Principal coordinate analysis (PCoA) of mouse intact sperm tsRNA/rsRNA data showing that PANDORA-seq, but not traditional sncRNA-seq, identified a clear 'aging cliff' separation during the 50–70-week transition in mouse sperm, marked by a dramatic shift in tsRNA/rsRNA composition. Axis 1: the first principal coordinate; Axis 2: the second principal coordinate. (**C**) PCoA on sperm head tsRNA/rsRNA data similarly show clearer demarcation during the 50–70-week transition using PANDORA-seq, compared to traditional sncRNA-seq. The PCoA presented in panel (**B**, **C**) was performed based on the expression profile of the individual tsRNA/rsRNA families. (**D**, **E**) Coverage plots of illustrative tsRNAs and rsRNAs from (**D**) intact sperm and (**E**) sperm heads mapped to their parent sequences across age groups. The reads mapping also shows the location from which the tsRNAs and rsRNAs are derived from the mature tRNAs and rRNAs. The solid curves indicate the mean of reads per million (RPM), while the shaded bands indicate the standard error of the mean. (**F**) Schematic illustrating de-membranation of sperm and the image of purified sperm heads (depleted of tails and mitochondria), with pie chart showing the composition of sncRNAs in sperm heads: predominantly genomic rsRNAs (73.7%) and tsRNAs (26.0%), with minor mitochondrial tsRNAs (0.14%) and rsRNAs (0.11%). (**G**) Correlation heatmap of all genomic tsRNA/rsRNA and mitochondrial tsRNA/rsRNA in the de-membranated sperm heads. The colors in the heatmap represent the intensity of co-expression (i.e., Spearman's rank correlation coefficient) between the sncRNAs: red indicates positive co-expression while blue indicates negative co-expression. Notably, the highly positively correlated clusters in the center square area (*Fisher*'s exact test: $P = 9.4 \times 10^{-8}$) are largely overlapped with mt-tsRNAs/rsRNAs, marked in orange color. The detailed identity of each tsRNAs and rsRNA category is shown in Fig. EV2. (**H**) Separated PCoAs for genomic tsRNAs, genomic rsRNAs, mitochondrial tsRNAs, and mitochondrial rsRNAs in sperm heads across the aging process. Mitochondrial tsRNAs and rsRNAs show demarcation power similar to genomic tsRNAs/rsRNAs, despite their relatively low expression level. The PCoA was performed based on the expression profile of the individual sncRNA species. G-tsRNA (genomic tsRNA), Mt-tsRNA (mitochondrial tsRNA), G-rsRNA (genomic rsRNA), Mt-rsRNA (mitochondrial rsRNA). Source data are available online for this figure.

The consistent detection of mt-tsRNAs and mt-rsRNAs in de-membranated sperm heads also strongly suggests that these RNA fragments are transported from the mitochondria to the nucleus, potentially serving as a mechanism for mitochondria-nucleus communication that influences the sperm aging process, a possibility that warrants further investigation.

Sperm-head rsRNAs exhibit an age-dependent length shift in mice

Beyond the general aging cliff, PANDORA-seq analysis of sncRNA subtypes in mouse sperm revealed an unexpected age-related shift: the relative abundance of longer rsRNAs increased while that of shorter rsRNAs decreased (Fig. 2A,C)—based on the calculation of the association of expression (*RPM*) of each RNA length category with age, which we termed as aging index (I_a) (Fig. 2A). This length shift in rsRNAs is specific to sperm heads (Fig. 2A), not whole sperm (Fig. 2B), and is prominent in rsRNAs derived from 28S- and 18S-rRNAs (Fig. 2A), which dominate the rsRNA pool. Similar trends are also observed in mitochondrial rsRNAs derived from 12S-rRNA and 16S-rRNA (Fig. EV3A). In contrast, tsRNAs did not show such an age- associated length-shift pattern overall (Fig. EV4).

The rsRNA length shift suggests that aged sperm have a reduced ability to process longer rsRNAs into shorter fragments, possibly due to oxidative-stress-induced changes that alter the activity or abundance of the responsible enzymes during aging. Supporting this, we identified regions where longer rsRNAs accumulate, and shorter rsRNAs diminish during aging, such as in the 4660–4730 nt of 28S-rRNA (Fig. 2D). Notably, these longer 28S-rsRNAs are among the most abundant sncRNAs showing significant age-related changes. This finding raises the possibility that longer and shorter rsRNAs play distinct roles, potentially contributing to reduced fertility or offspring health issues linked to aged sperm.

A conserved rsRNA length shift marks human sperm aging

Given PANDORA-seq's success in detecting aging signatures in mouse sperm, we next applied it to human sperm from two independent cohorts: a longitudinal cohort of 8 donors, each providing two samples collected over 6–23 years apart, with ages ranging from 34 to 68 years (cohort-1) (Fig. 3A); and a cross-sectional cohort of 47 donors aged 25–51 years (cohort-2) (Fig. 3B). For both cohorts, we isolated RNA from de-membranated sperm heads for two reasons: (1) mouse data showed that sperm heads are enriched with aging-related signals, including the rsRNA length shift, and (2) human sperm variability—such as viscosity, debris, or cytoplasmic droplets—can confound RNA purity, making sperm heads a more reliable source of uncontaminated RNA.

Analysis of PANDORA-seq data from both human cohorts revealed a consistent age-related shift in rsRNA length, mirroring the trends observed in mice (e.g., longer rsRNAs increasing and shorter decreasing in relative abundance). This shift was evident in total rsRNAs (Fig. 3A,B), and specifically for rsRNAs derived from 18S- and 28S-rRNAs (Fig. 3A,B). Mitochondrial rsRNAs also showed a similar trend but with weaker statistical significance (Fig. EV3B,C), likely due to their lower abundance and fewer sequencing reads, compounded by the inherent genetic and environmental variability of human samples. Nonetheless, these findings suggest that the rsRNA length shift is an evolutionarily conserved feature of aging across mice and humans. This shift may stem from age-related changes in enzymatic activity or levels, potentially linked to altered mitochondrial function and oxidative stress—common factors in sperm aging (Aitken, 2023). Importantly, it is well established that oxidative stress controls the fragmentation of tRNA and rRNA by regulating the recruitment and activity of specific ribonucleases (Chen et al, 2021). Such alterations in these processes impact the biogenesis and/or processing of tsRNAs/rsRNAs and reshape the "sperm RNA code," which may impact embryo development and offspring phenotypes as a functional readout of sperm aging.

Age-mimicking sncRNA profiles reprogram embryonic metabolic and neurodegenerative pathways

To investigate the functional significance of age-related changes in sperm sncRNAs, we selected a group of tsRNAs and rsRNAs that exhibited high expression level with the most significant differences in expression shared in sperm and sperm heads during mouse aging

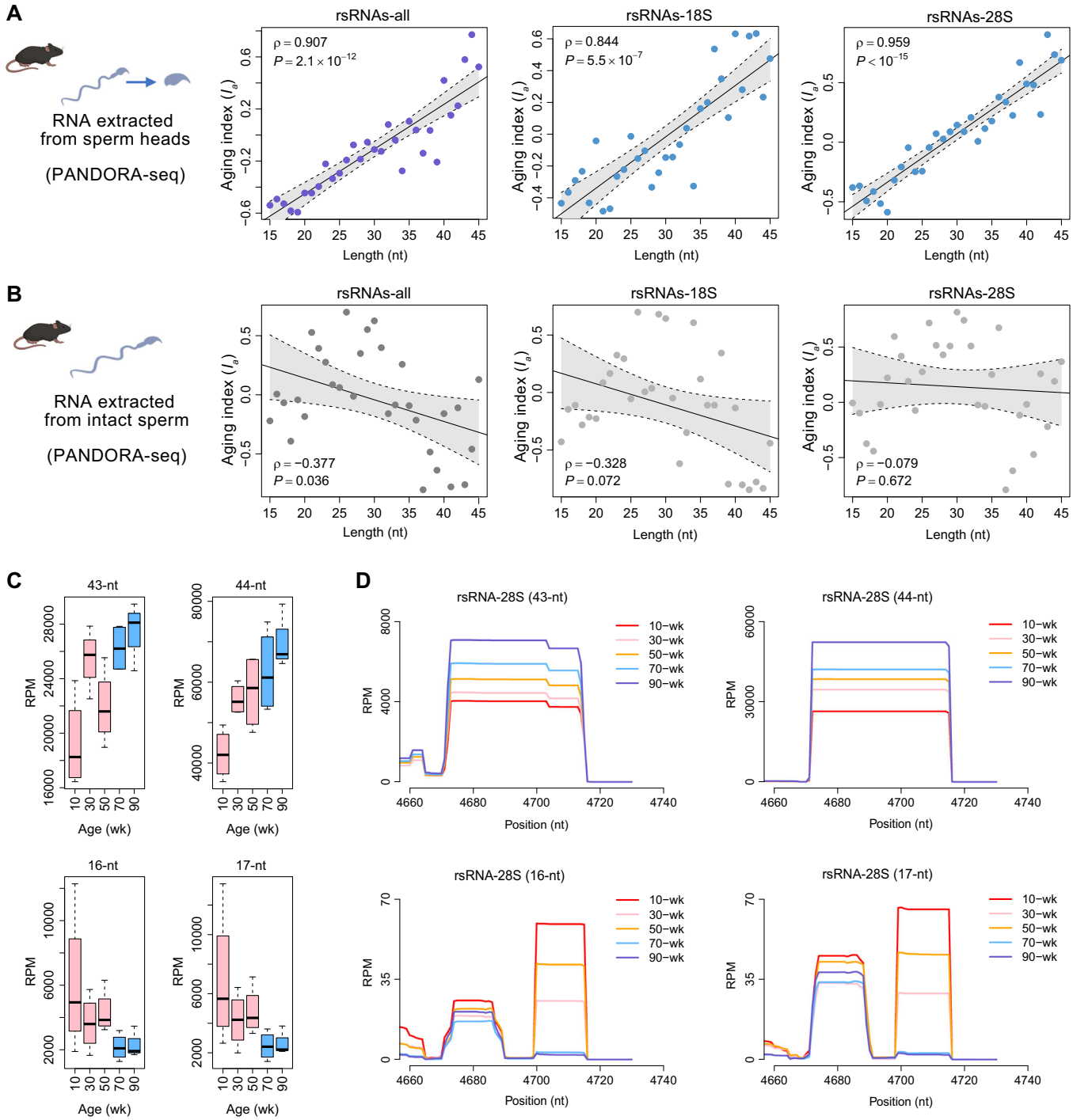

(Fig. 4A). These RNAs were combined into cocktails representing "young" and "old" sperm profiles (see Fig. 4A and Methods for detailed composition). We transfected the RNA cocktails into mouse embryonic stem cells (mESCs), chosen as a model system because they resemble early embryonic cells potentially influenced by sperm-derived sncRNAs during pre-implantation development. To assess the functional impact of these age-related sncRNA profiles, we performed RNA-seq analysis at 24 h post-transfection in mESCs, a time point at which no apparent growth or morphological changes were observed.

As a result, principal component analysis (PCA) revealed clear separation of gene expression profiles among the vehicle (mock-transfected), young-combo, and old-combo groups (Fig. 4B). Both RNA-treated groups differed substantially from the vehicle, with overlap in altered genes as shown in Venn diagram (Fig. 4C; Tables EV2–5) yet also showed distinct gene expression profiles between

Figure 2. Discovery of age-related length shift of rsRNAs in mouse sperm heads.

(**A**) Age-related length shift of total rsRNAs, 18S-derived rsRNAs, and 28S-derived rsRNAs in mouse sperm head. For each RNA length category, we calculated the association of expression (*RPM*) with age (*Spearman*'s rank correlation), which we termed as aging index (I_a). Each dot represents the value of I_a for the corresponding length. The scatter plots demonstrate the relationship between I_a and RNA length, which was measured by *Spearman*'s rank correlation coefficient (ρ) and the corresponding *P* value. The solid lines depict linear regression fits. Strong positive correlations were observed between I_a and RNA length across all the categories (i.e., total rsRNA and 18S-/28S-derived rsRNAs). (**B**) Relationship between I_a and RNA length in mouse intact sperm. Weak negative correlation (in total rsRNA) or no correlations (in 18S-derived and 28S-derived rsRNAs) were observed regarding length shifts with age. (*Spearman*'s rank correlation). (**C**) Boxplot of *RPM* for different rsRNA lengths (43-nt, 44-nt, 16-nt, and 17-nt) from total rsRNAs across mouse age groups (10–90 weeks). The bold horizontal line indicates the median of the data. The lower and upper boundaries of the box indicate the 25th percentile (Q1) and 75th percentile (Q3) of the data, respectively. Accordingly, the interquartile range (IQR) is Q3-Q1. The lower and upper whiskers indicate the most extreme data points that fall within Q1-1.5 × IQR and Q3 + 1.5×IQR, respectively. (**D**) Coverage plots of the rsRNA fragments mapped to 28S-rRNA (4660 nt - 4730 nt), stratified by length (43-nt, 44-nt, 16-nt, and 17-nt). Lines represent the mean coverage level at each position, illustrating the accumulation of longer fragments and diminution of shorter ones with advancing age. Source data are available online for this figure.

the old-combo and young-combo, as shown in the heatmap (Fig. 4D; Tables EV6 and 7).

Further Gene Ontology analyses of the differentially expressed genes between young-combo and old-combo groups revealed that the old-combo induced upregulation of genes involved in metabolic pathways (e.g., fatty acid metabolism, carbon metabolism, glycolysis/gluconeogenesis), mitochondrial function (oxidative phosphorylation, mitophagy), and neurodegenerative diseases (e.g., Parkinson's disease, Alzheimer's disease, Huntington's disease) (Fig. 4E; Table EV8). These altered pathways align with offspring phenotypes associated with aged sperm or induced by zygotic injection of RNAs from aged sperm, including metabolic and neurological disorders (Guo et al, 2021; Mao et al, 2022). Interestingly, recent reports have shown that dysregulated sperm RNAs under high-fat diet conditions can impact the metabolic gene expression in the early embryo (Chen et al, 2016a; Tomar et al, 2024), especially impacting two-cell embryo's oxidative phosphorylation pathway (Cai and Chen, 2024; Tomar et al, 2024), suggesting an intertwined relationship between aging and dietary factors on sperm quality and the subsequent mitochondrial functions in embryo development and offspring health. Our findings here provide proof-of-principle evidence that different combinations of tsRNAs/rsRNAs mimicking young versus old sperm status can profoundly affect mESC gene expression, the mechanistic details of which await further investigations, and the RNA modification status of tsRNAs/rsRNAs may further complicate the situation (Chen and Zhou, 2023; Kuhle et al, 2023; Shi et al, 2022).

Discussion

Our discovery of the sncRNA-based "aging cliff" in mouse sperm characterizes a striking shift in tsRNA and rsRNA profiles within a specific age range. However, what drives this sudden transition? Studies of other systems, like blood proteins, reveal similar cliff-like aging patterns (Ding et al, 2025; Shen et al, 2024), reinforcing the idea that aging can leap forward at critical time windows. Does this suggest that molecular changes occur abruptly at a certain stage? Or could subtle, progressive changes act as "forerunner signals" that set the stage for the later, larger shift? In our data, despite the overall tsRNA/rsRNA aging cliff, some sperm tsRNA/rsRNA levels indeed change gradually; in particular, the rsRNA length shift progresses steadily during mouse aging (Fig. 2D). Our mESC transfection experiments further show that sncRNAs exhibiting these gradual changes, when introduced, trigger substantial transcriptomic responses, particularly in mitochondrial function pathways (Fig. 4E). These pathways, central to cellular aging, might amplify subtle sncRNA shifts into the pronounced cliff we observe, suggesting a model where incremental changes (Shi et al, 2015) (e.g., the linear trends of quantity and length shift of individual rsRNAs) potentially driven by accumulating oxidative stress, cascade into a transformative cliff effect.

The source of these sperm sncRNA changes remains an open question. They may arise from altered biogenesis and regulation during testicular germ cells development, epididymal sperm maturation, or from sncRNAs delivered by somatic cells reflecting systemic aging, or from a combination of these factors (Chen et al, 2016b; Conine and Rando, 2022; Cui et al, 2025; Nie et al, 2022). While the precise upstream trigger of aging is unclear, gradual oxidative stress—a hallmark of aging in the testis, sperm, and other systems—likely plays a significant role. Oxidative stress is known to modulate tRNA and rRNA fragmentation by regulating ribonuclease activity at specific positions (Chen et al, 2021; Thompson et al, 2008), potentially driving the observed shifts in tsRNA and rsRNA level and length, the details of which warrant further investigations.

Finally, the mechanisms by which sperm tsRNAs and rsRNAs regulate gene expression in mESCs and/or early embryonic development remain underexplored. While certain tsRNAs and rsRNAs can use miRNA-like mechanisms to linearly bind to their RNA targets, with or without the involvement of AGO proteins (Chen and Zhou, 2023), other tsRNAs and rsRNAs may fold into specific structures, to bind to specific proteins to exert their functions in an aptamer-like manner (Chen and Zhou, 2023; Kuhle et al, 2023). These modes of action can be further fine-tuned by specific RNA modifications, which can regulate sncRNA stability (Zhang et al, 2018), linear binding efficiency to their RNA targets (Su et al, 2022) or protein partners (Guzzi et al, 2018), enabling increased functional versatility. Due to the complex set of RNA modifications carried by tsRNAs and rsRNAs, one limitation of our transfection experiment (Fig. 4A) is that these synthetic tsRNAs and rsRNAs may not function in a way that fully mimics their in vivo status. Future methods like nanopore-based sequencing (Lucas et al, 2023) and advanced mass spectrometry-based methods (Yuan et al, 2024), after proper optimization (Shi et al, 2022), may provide detailed RNA modification maps for each sncRNA, and thus guide more precise functional investigations.

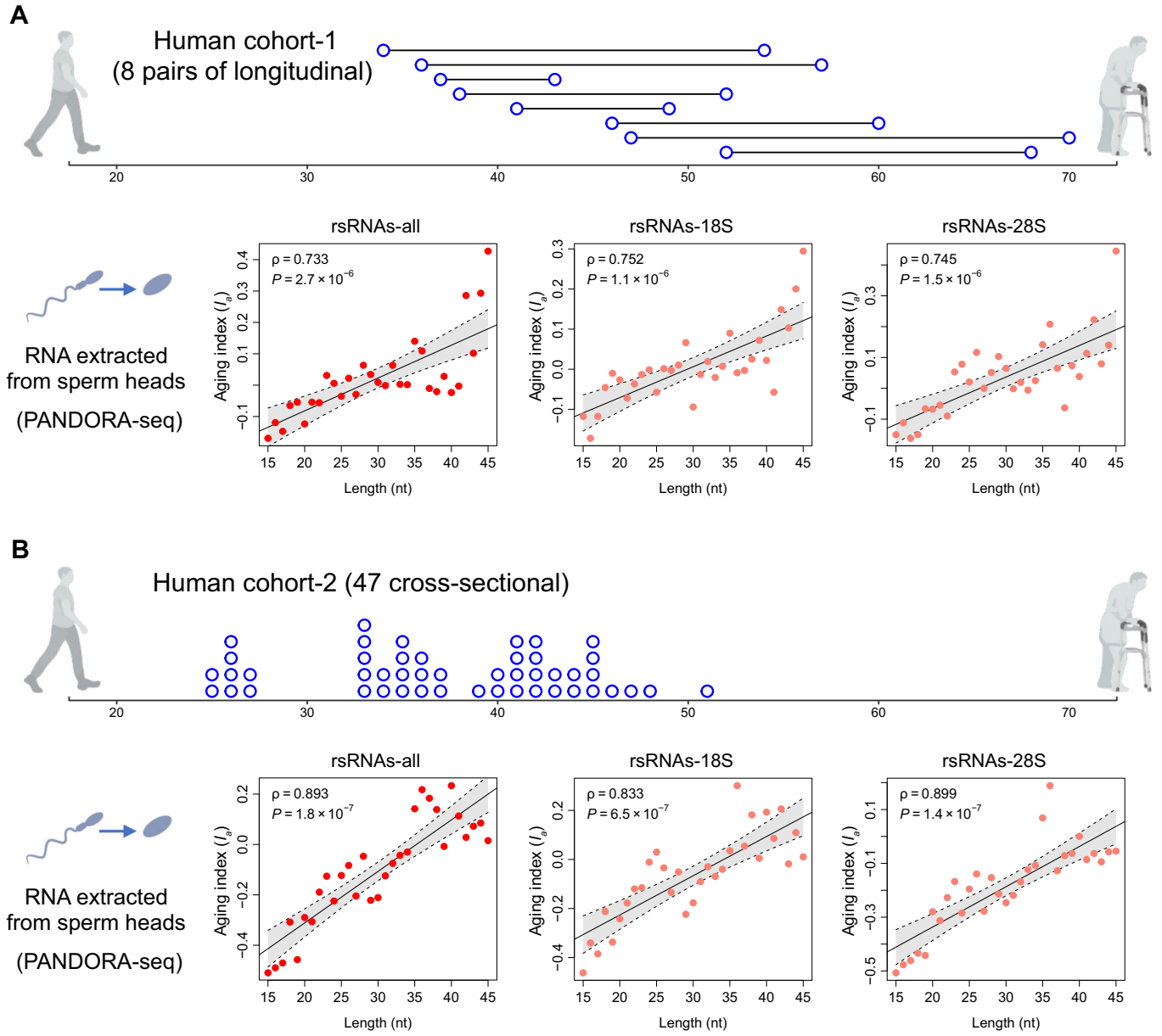

Figure 3. Conserved age-related length shift of rsRNAs in human sperm cohorts.

(**A**) Age-related length shift of total rsRNAs, 18S-derived rsRNAs, and 28S-derived rsRNAs in human sperm head from cohort-1. Upper panel shows the schematic of the longitudinal human cohort-1 (eight donors, each with paired samples over 6–23 years apart, with ages ranging from 34 to 68 years. The blue hollow dots connected by line represent each individual donor. RNA sample was extracted from de-membranated sperm heads followed by PANDORA-seq. For each RNA length category, we calculated the association of expression (RPM) with age (Spearman's rank correlation), which we termed as aging index (I_a). Each dot represents the value of I_a for the corresponding length. The scatter plots demonstrate the relationship between I_a and RNA length, which was measured by Spearman's rank correlation coefficient (ρ) and the corresponding P value. The solid lines depict linear regression fits. (**B**) Age-related length shift of total rsRNAs, 18S-derived rsRNAs, and 28S-derived rsRNAs in human sperm head from the cross-sectional cohort-2 (47 donors with ages ranging from 25 to 51 years). The blue hollow dots represent individual donors. The scatter plots demonstrate the consistent relationship between I_a and RNA length in cohort-2 .Both human cohorts show conserved age-related length shift of rsRNAs (total rsRNAs, rsRNA-18S, and rsRNA-28S), which mirrors the observation in mouse aging. (Spearman's rank correlation). Source data are available online for this figure.

In summary, leveraging the advances of PANDORA-seq, we have unveiled a novel sperm aging landscape in mice and humans. The conserved rsRNA length shift across species signals the potential for sncRNA-based biomarkers to guide informed reproductive decisions. Looking ahead, tracing the origins of these sncRNA changes and identifying the RNA-processing enzymes that control tsRNA and rsRNA biogenesis and length could unlock transformative interventions. These directions may not only predict but also prevent the transmission of age-related disorders to offspring, heralding a new era in reproductive health where a deeper understanding of the "sperm RNA code" helps shape healthier generations.

Methods

Reagents and tools table

Reagent/resource	Reference or source	Identifier or catalog number
Experimental models		
C57BL/6J mice	The Jackson Laboratory	IMSR_JAX:000664
Mouse embryonic stem cell (v6.5)	Dr. Sihem Cheloufi Lab	
Recombinant DNA		
Antibodies		
Oligonucleotides and other sequence-based reagents		
tsRNA-Pro-CGG: 5′/Phos/ rGrGrCrUrCrGrUrUrGr GrUrCrUrArGrGrGrGrUrArUr GrArUrUrCrUrCrGrCrUrU-2′3 c-Phos	ChemGene	Customer service, Lot#: L193598-1
28S-rsRNA 44-nt: 5′/Phos/ rCrUrCrGrCrUrGrCr GrArUrCrUrArUrUrGrArArArGr UrCrArGrCrCrCrUrCrGrArCrArCrAr ArGrGrGrUrU rUrG-2′3 c-Phos	ChemGene	Customer service, Lot#: L193598-2
28S-rsRNA 17-nt: 5′/Phos/ rCrUrCrGrArCrArCrArAr GrGrGrUrUrUrG-2′3 c-Phos	ChemGene	Customer service, Lot#: L193598-3
tsRNA-Arg-CCT: 5′/Phos/ rArGrGrGrArUrUrGrUrGrGr GrUrUrCrGrArGrUrCrCrCr ArUrCrUrGrGrGrUrGrC-2′3 c-Phos	ChemGene	Customer service, Lot#: L193598-4
5S-rsRNA: 5′/Phos/rUrGr GrGrArGrArCrCrGrCrCrUrGr GrGrArArUrArCrCrGrGrGr UrGrCrUrGrUrArGrGrCrU-2′3 c-Phos	ChemGene	Customer service, Lot#: L193598-5
Chemicals, Enzymes and other reagents		
AlkB enzyme	Addgene	228218
T4PNK	New England Biolabs	M0201L
Lipofectamine Stem Transfection Reagent	Invitrogen	STEM00003
NEBNext® Small RNA Library Prep Set for Illumina® (Multiplex Compatible)	New England Biolabs	E7330S
TRIzol	Invitrogen	15596018
10 X TBE	Invitrogen	AM9863
2X RNA loading dye	New England Biolabs	B0363S
Urea	Invitrogen	AM9902
Ammonium persulfate	Sigma-Aldrich	A3678-25G
TEMED	Thermo Fisher Scientific	BP150-100
SYBR Gold	Invitrogen	S11494
3 M Sodium acetate	Invitrogen	AM9740
RNase inhibitor	New England Biolabs	M0314L
Linear acrylamide	Invitrogen	AM9520
Isopropanol	Fisher Scientific	BP2618-212
Chloroform	Alfa Aesar	J67241
Proteinase K Solution	Invitrogen	25530049
0.5 M EDTA	Invitrogen	AM9261
10% SDS	Sigma-Aldrich	71736-100 ML
10% Triton X-100	Sigma-Aldrich	93443-100 ML
10XPBS	Gibco	70013032
Tris-HCl, pH 8.0	Invitrogen	AM9855G
Nuclease-free water	Invitrogen	10977-015
Ethanol	Koptec	Cat. No. V1001
Low-range ssRNA ladder	New England Biolabs	N0364S
14–30 ssRNA Ladder Marker	Takara	3416
10 mM ATP solution	New England Biolabs	P0756S
HEPES (pH 8.0)	Gibco	15630080
Ferrous ammonium sulfate	Sigma-Aldrich	215406
α-ketoglutaric acid	Sigma-Aldrich	K1128-25G
Bovine serum albumin (BSA)	Sigma-Aldrich	A7906-500G
Knock-out DMEM	Gibco	10829
Fetal bovine serum (FBS)	Gibco	10437; Lot-2190737RP
GlutaMAX Supplement	Gibco	35050061
100 X Streptomycin solution	Gibco	15140
Non-essential amino acids	Gibco	11140
2-Mercaptoethanol	Gibco	21985
ESGRO® Recombinant Mouse LIF Protein	Sigma-Aldrich	ESG1106
Software		
SPORTS1.1	https://github.com/junchaoshi/sports1.1	
Kallisto tool	https://github.com/pachterlab/kallisto	
edgeR	https://bioconductor.org/packages/release/bioc/html/edgeR.html	
DAVID tool	https://davidbioinformatics.nih.gov/	
Illustrator software	Adobe Inc.	
R	https://www.r-project.org/	
Other		
Illumina NovaSeq X plus	Illumina	

Animals

Animal experiments were conducted under the protocol and approval of the institutional animal care and use committees of the University of California, Riverside. Mice were given access to food and water ad libitum and were maintained on a 12 h light/12 h dark artificial lighting cycle. Mice were housed in cages at a temperature of 22–25 °C, with 40–60% humidity.

Mouse sperm samples during aging

Mature sperm were collected from the cauda epididymis of male C57BL/6J mice, aged at 10, 30, 50, 70, and 90 weeks, and then were released into 5 ml of phosphate-buffered saline (PBS). This mixture was then incubated at 37 °C for 15 min, followed by filtration through a 40-μm cell strainer to remove tissue debris. To eliminate somatic cell contamination, the filtered sperm were incubated with a somatic cell lysis buffer (comprising 0.1% sodium dodecyl sulfate (SDS) and 0.5%

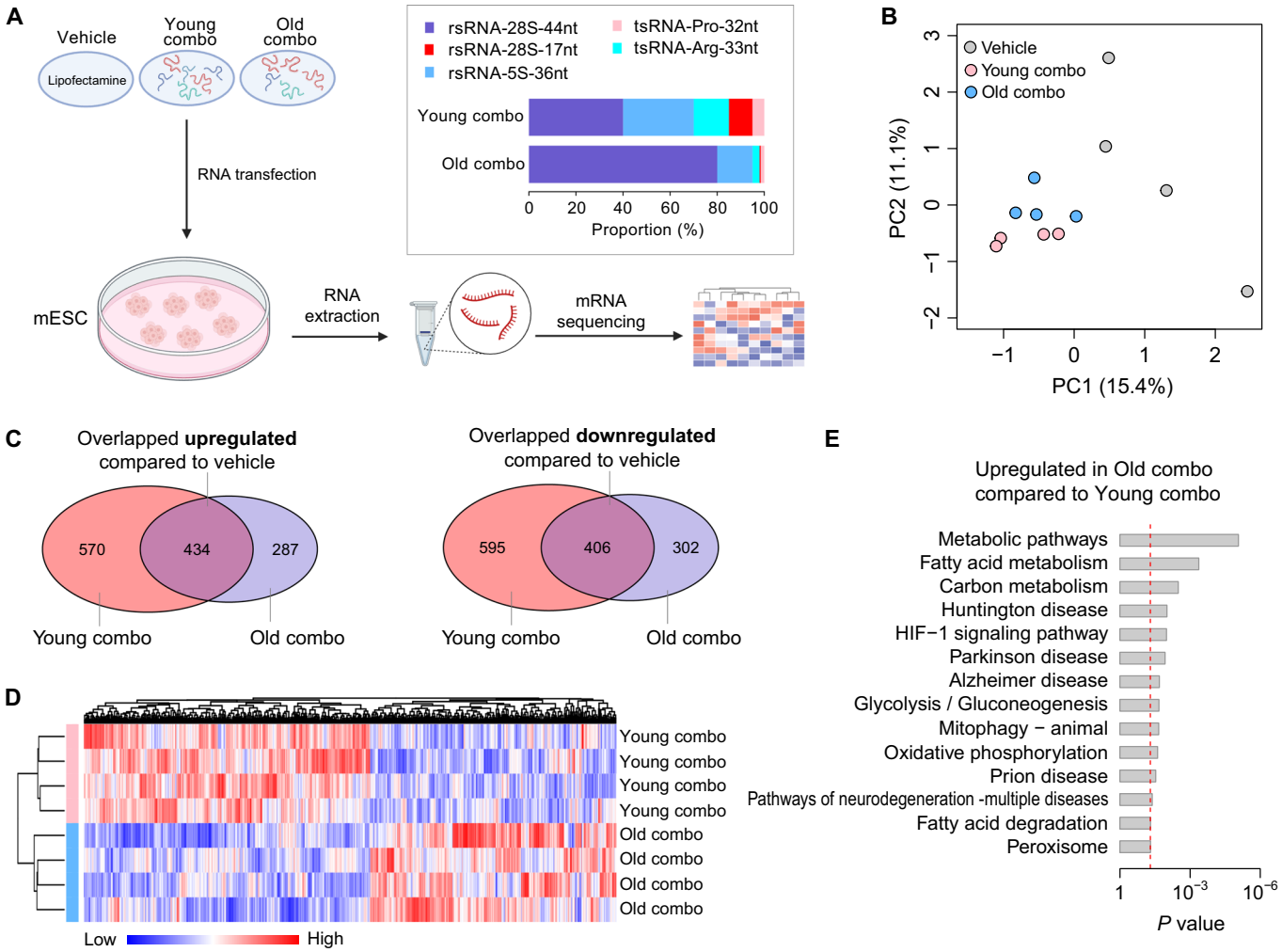

Figure 4. Functional impact of age-related sperm sncRNAs on transcriptomic profiles in mouse embryonic stem cells.

(A) Schematic of the experimental design: Synthetic RNA cocktails mimicking "young" or "old" sperm sncRNA profiles (composed of selected tsRNAs and rsRNAs with significant age-related differences in expression and length) were transfected into mESCs via lipofectamine, followed by RNA extraction 24 h post transfection, and mRNA sequencing analysis. Bar plots show the proportional composition (%) of key sncRNAs in the young combo (28S-rsRNA-44nt (40%); 28S-rsRNA-17nt (10%); 5S-rsRNA-36nt (30%); tsRNA-Arg-33nt (15%); tsRNA-Pro-32nt (5%)) and old combo (28S-rsRNA-44nt (80%); 28S-rsRNA-17nt (0.5%); 5S-rsRNA-36nt (15%); tsRNA-Arg-33nt (3%); tsRNA-Pro-32nt (1.5%)). **(B)** Principal component analysis (PCA) of the transcriptomic profile from mESCs transfected with vehicle, young combo, or old combo RNAs ($n = 4$ per group). **(C)** Venn diagrams illustrating overlap in upregulated (left) and downregulated (right) genes in young combo and old combo groups compared to the vehicle. **(D)** Heatmap of differentially expressed genes between young combo and old combo groups, showing clustering of replicates ($n = 4$ per group). **(E)** The top KEGG pathways ($P < 0.05$) associated with the upregulated genes in the old combo group relative to the young combo group. The red dashed line indicates the significance level of $\alpha = 0.05$. (Modified Fisher's exact test). Source data are available online for this figure.

Triton X-100 in nuclease-free water) for 40 min on ice. Subsequently, the sperm were pelleted by centrifugation at 600×*g* for 5 min. The sperm pellet was then resuspended in 10 ml PBS, washed, and centrifuged twice at 600×*g* for 5 min each time. Finally, RNA isolation was performed on the precipitated sperm. Sperm age groups and sample information for sequencing are included in Table EV9.

Human sperm samples

Study participants gave informed consent for semen samples to be used for research under University of Utah IRB # 0012049. In longitudinal cohort (cohort-1) with known fertility, eight donors each provided two semen samples across an interval of 6–23 years, with the ages at which they provided these samples detailed in Fig. 3A; Table EV10. Smoking and alcohol use were exclusion criteria for donors in cohort-1. In the cross-sectional cohort (cohort-2), 47 individuals are included (25–51 years) detailed in Fig. 3B and Table EV11. Two participants in cohort-2 self-reported smoking (one regularly smokes cigarettes, the other smokes 1–2 cigars/month), and 24 self-reported some alcohol consumption (1–2 times/week), with no heavy drinkers included. Smoking and alcohol use information of cohort-2 is included in Table EV11. All semen samples were collected in our Andrology Laboratory (University of Utah School of Medicine) under the following quality criteria: (i) sperm concentration $\geq 15 \times 10^6$/ml; (ii) progressive motility ≥32% (iii) normal morphology ≥14%. All semen samples were collected

by masturbation following 2–5 days of sexual abstinence and were subsequently cryopreserved in commercially available sperm cryopreservation media (TYB media; Irvine Scientific) and stored in liquid nitrogen until use in the study. The sizes of human cohorts are chosen based on the resource available at our disposal at the time of study.

Sperm head isolation

Sperm head isolation was according to established protocols (Shi et al, 2025). For mouse sperm head, mature sperm were released from the cauda epididymis of male mice into 5 mL PBS and incubated at 37 °C for 15 min. For human sperm head, 1 mL frozen semen sample were thaw at 37 °C for 2 min then added to 4 mL PBS followed by incubation at 37 °C for 15 min. The suspension was filtered through a 40-μm cell strainer to remove tissue debris and centrifuged at 3000×*g* for 5 min. Pelleted sperm were incubated in lysis buffer (10 mM Tris-HCl, pH 8.0; 10 mM EDTA; 50 mM NaCl; 2% SDS; and 75 μg/mL proteinase K) for 15 min at room temperature, then centrifuged at 3000×*g* for 5 min. The pellet was collected, resuspended, washed in 5 ml PBS and centrifuged at 600×*g* for 5 min, repeated twice. Sperm head purity was confirmed by light microscopy before RNA extraction. For RNA isolation, add at least 500 μL TRIzol to the pellet and pass the suspension repeatedly through a 27 G needle until fully lysed with no visible precipitate.

Total RNA isolation

TRIzol reagent (1 ml; Invitrogen, Cat. No. 15596018) was added to microtubes containing sperm and sperm head samples, followed by uniform vortexing. The samples were then incubated at room temperature for 5 min. To each milliliter of the sample, 200 μl of chloroform (Alfa Aesar, Cat. No. J67241) was added, vortexed for 15 s, incubated at room temperature for 2 min, and then centrifuged at 12,000×*g* for 15 min at 4 °C. The aqueous phase was transferred to a new microtube and mixed with an equal volume of isopropanol (Fisher Scientific, Cat. No. BP2618-212). After mixing, the samples were incubated at room temperature for 10 min, followed by centrifugation at 12,000×*g* for 10 min at 4 °C. The supernatant was discarded, and the pellet was washed with 1 ml of 75% ethanol (Koptec, Cat. No. V1001), then centrifuged at 7500×*g* for 5 min at 4 °C. The supernatant was removed, and the pellet was air-dried for 5 min. Finally, the pellet was resuspended in nuclease-free water, quantified, and either stored at −80 °C or used for further analyses.

Isolation of 15–50 nt RNA fraction from total RNAs

The RNA sample, mixed with an equal volume of 2× RNA loading dye (New England Biolabs; B0363S), was incubated at 75 °C for 5 min. The mixture was loaded into 15% (wt/vol) urea polyacrylamide gel (10 ml mixture containing 7 M urea (Invitrogen; AM9902), 3.75 ml Acrylamide/Bis 19:1, 40% (Ambion; AM9022), 1 ml 10× TBE (Invitrogen; AM9863), 1 g l^{-1} ammonium persulfate (Sigma–Aldrich; A3678-25G) and 1 ml l^{-1} TEMED (Thermo Fisher Scientific; BP150-100)). The gel was run in a 1× TBE running buffer at 200 V until the bromophenol blue reached the bottom of the gel. After staining with SYBR Gold solution (Invitrogen; S11494), the gel that contained small RNAs of 15–50 nucleotides was excised based on small RNA ladders (New England Biolabs (N0364S) and Takara (3416)) and eluted in 0.3 M sodium acetate (Invitrogen; AM9740) and 100 U ml^{-1} RNase inhibitor (New England Biolabs; M0314L) overnight at 4 °C. The sample was then centrifuged for 10 min at 12,000×*g* (4 °C). The aqueous phase was mixed with pure ethanol, 3 M sodium acetate and linear acrylamide (Invitrogen; AM9520) at a ratio of 3:9:0.3:0.01. Then, the sample was incubated at −20 °C for 2 h and centrifuged for 25 min at 12,000×*g* (4 °C). After removing the supernatant, the precipitation was resuspended in nuclease-free water, quantified and stored at −80 °C or used for further processing. The RNAs were then separated into two halves, one for PANDORA-seq, and the other for traditional sncRNA-seq.

PANDORA-seq and traditional sncRNA-seq

PANDORA-seq

RNA fragments ranging from 15 to 50 nucleotides (nt) were incubated in a 50 μL reaction mixture containing 5 μL 10× PNK buffer (New England Biolabs; B0201S), 1 mM ATP (New England Biolabs; P0756S), 10 U T4PNK (New England Biolabs; M0201L) at 37 °C for 20 min. Following this incubation, the reaction mixture was added to 500 μL of TRIzol reagent to perform the RNA isolation procedure. Then the purified RNA was incubated in 50 μL reaction mixture containing 50 mM HEPES (pH 8.0) (Gibco (15630080) and Alfa Aesar (J63578)), 75 μM ferrous ammonium sulfate (pH 5.0), 1 mM α-ketoglutaric acid (Sigma–Aldrich; K1128-25G), 2 mM sodium ascorbate, 50 mg l^{-1} bovine serum albumin (Sigma–Aldrich; A7906-500G), 4 μg ml^{-1} AlkB, 2,000 U ml^{-1} RNase inhibitor at 37 °C for 30 min. Subsequently, this reaction mixture was also added to 500 μL of TRIzol reagent to perform the RNA isolation procedure, followed by small RNA library construction and deep sequencing.

Traditional sncRNA-seq

15–50 nt RNA fraction was directly processed for small RNA library construction and deep sequencing.

Small RNA library construction and deep sequencing

The adapters were sourced from the NEBNext Small RNA Library Prep Set for Illumina (New England Biolabs, Catalog No. E7330S) and were ligated in sequence. First, a 3′ adapter was added under the following reaction conditions: incubation at 70 °C for 2 min, followed by 16 °C for 18 h. Subsequently, a reverse transcription primer was introduced under these conditions: 75 °C for 5 min, 37 °C for 15 min, and then 15 °C for 15 min. Next, a 5′ adapter mix was added, with the reaction conditions set at 70 °C for 2 min and then 25 °C for 1 h. First-strand cDNA synthesis proceeded at 70 °C for 2 min and then at 50 °C for 1 h. PCR amplification was carried out to enrich the cDNA fragments, utilizing the PCR Primer Cocktail and PCR Master Mix under the following conditions: an initial denaturation at 94 °C for 30 s; followed by 14–23 cycles of denaturation at 94 °C for 15 s, annealing at 62 °C for 30 s, and extension at 70 °C for 15 s; with a final extension at 70 °C for 5 min and then a hold at 4 °C. The libraries were then amplified and sequenced using the PE100 RUN configuration on Illumina NovaSeq X Plus platform by the University of California, San Diego IGM Genomics Center. The summaries of sequencing datasets for mouse (Table EV9) and human (Tables EV10 and 11) samples are provided along with each sample's age information.

Processing the PANDORA-seq and traditional sncRNA-seq data

We used the *SPORTS* tool (v1.1) (Shi et al, 2018) to annotate and summarize the PANDORA-seq data and traditional sncRNA-seq with one mismatch tolerance. The "summary" files generated by *SPORTS* were used to quantify sncRNA read counts and reads per million (RPM) to measure the expression of the individual sncRNAs categories, including tsRNAs, rsRNAs, and miRNAs. For tsRNAs, only the RNA species derived from mature tRNAs were included for further analysis.

RNA-seq transcriptomic data analysis

The *kallisto* tool (Bray et al, 2016) was applied to quantify genome-wide gene expression from the RNA-seq data. The read count matrix was further analyzed using the *edgeR* tool (Robinson et al, 2010) to identify the differentially expressed genes. In brief, the *TMM* method was employed for data normalization. The likelihood ratio test was used to prioritize the differentially expressed genes. The genes with $P < 0.05$ were deemed differentially expressed. The *DAVID* tool (Sherman et al, 2022) was used to identify the KEGG pathways associated with the differentially expressed genes.

Small RNA transfection into mouse embryonic stem cells (mESCs)

Before transfection, 5×10^6 V6.5 mESCs were seeded into each well of 0.2% gelatin-coated six-well plate and incubated overnight (~16 h) with mESC media consisting of KO-DMEM (Gibco; 10829) supplemented with 15% FBS (Gibco; 10437; Lot-2190737RP), 2 mM GlutaMAX (Gibco; 35050), 100 U ml^{-1} penicillin (Gibco; 15140), 100 µg ml^{-1} streptomycin (Gibco; 15140), 100 uM non-essential amino acids (Gibco; 11140), 55 µM 2-mercaptoethanol (Gibco; 21985) and 1000 U ml^{-1} LIF (Sigma-Aldrich; ESG1106). The transfection complex was prepared as follows: 4 µL of small RNA cocktail (100 µM) with 8 µL Lipofectamine™ Stem Reagent and 188 µL Opti-MEM was mixed by vortexing and incubated at room temperature for 15 min. The media was discarded, and 1800-µL fresh mESC media (excluding antibiotics) was added to the wells. About 200 µL lipofectamine–RNA transfection complex was then added to each well and incubated for 24 h at 37 °C under 5% CO_2. The final small RNA transfection concentration was 200 nM. For each transfection, four independent replicates were performed. Vehicle-only transfections were used as a control.

The small RNA cocktail groups are as follows:

Young-comb: 28S-rsRNA-44nt (80 nM); 28S-rsRNA-17nt (20 nM); 5S-rsRNA-36nt (60 nM); tsRNA-Arg-CCT (30 nM); tsRNA-Pro-CGG (10 nM)

Old-comb: 28S-rsRNA-44nt (160 nM); 28S-rsRNA-17nt (1 nM); 5S-rsRNA-36nt (30 nM); tsRNA-Arg-CCT (6 nM); tsRNA-Pro-CGG (3 nM)

The synthetic small RNA sequences are as follows:

tsRNA-Pro-CGG:

5'/Phos/rGrGrCrUrCrGrUrUrGrGrUrCrUrArGrGrGrGrUrArUrGrArUrUrCrUrCrGrCrUrU-2'3 c-Phos

tsRNA-Arg-CCT:

5'/Phos/rArGrGrGrArUrUrGrUrGrGrGrUrUrCrGrArGrUrCrCrArUrCrUrGrGrGrGrUrGrC-2'3 c-Phos

28S-rsRNA 44-nt:

5'/Phos/rCrUrCrGrCrUrGrCrGrArUrCrUrArUrUrGrArArArGrUrCrArGrCrCrCrUrCrGrArCrArCrArArGrGrGrUrUrUrG-2'3 c-Phos

28S-rsRNA 17-nt:

5'/Phos/rCrUrCrGrArCrArCrArArGrGrGrUrUrUrG-2'3 c-Phos

5S-rsRNA:

5'/Phos/rUrGrGrGrArGrArCrCrGrCrCrUrGrGrGrArArUrArCrCrGrGrGrUrGrCrUrArGrGrCrU-2'3 c-Phos

At 24 h post-transfection, total RNA from mESCs was extracted with TRIzol (per manufacturer's instructions) and subjected to transcriptome-wide RNA-seq using a polyA enrichment strategy (Novogene), followed by bioinformatic analyses for differential gene expression and pathway discovery, as described previously (Shi et al, 2021).

Statistical analyses

All the statistical analyses were conducted using the R programming platform. The *Spearman*'s rank correlation test, *Wilcoxon* test, and *Fisher*'s exact test were performed using the "cor.test", "wilcox.test", and "fisher.test" functions, respectively, with two-sided *P* values being computed. The *F*-statistic was computed by the "aov" function. The principal coordinate analysis (PCoA) was performed using the "pcoa" function within the "ape" package. The dissimilarity indices were computed using the "vegdist" function within the "vegan" package based on the "clark" method. The principal component analysis (PCA) was performed using the "dudi.pca" function within the "ade4" package. The co-expression and gene expression heatmaps were generated by the "heatmap.2" function within the "gplots" package. The hierarchical clustering was performed using the "complete" method with "euclidean" distance. The Venn diagrams were plotted using the "venn.diagram" function within the "vennDiagram" package.

Data availability

The sncRNA annotation pipeline *SPORTS* is available from GitHub (https://github.com/junchaoshi/sports1.1). RNA-seq datasets have been deposited in the Gene Expression Omnibus under the accession code GSE256182.

The source data of this paper are collected in the following database record: biostudies:S-SCDT-10_1038-S44318-025-00687-8.

Expanded view data, supplementary information, appendices are available for this paper at https://doi.org/10.1038/s44318-025-00687-8.

Peer review information

A peer review file is available at https://doi.org/10.1038/s44318-025-00687-8

References

Aitken RJ (2023) Male reproductive ageing: a radical road to ruin. Hum Reprod 38:1861–1871

Ashapkin V, Suvorov A, Pilsner JR, Krawetz SA, Sergeyev O (2023) Age-associated epigenetic changes in mammalian sperm: implications for offspring health and development. Hum Reprod Update 29:24–44

Bray NL, Pimentel H, Melsted P, Pachter L (2016) Near-optimal probabilistic RNA-seq quantification. Nat Biotechnol 34:525–527

Cai C, Chen Q (2024) Father's diet influences son's metabolic health through sperm RNA. Nature 630:571–573

Chen Q (2022) Sperm RNA-mediated epigenetic inheritance in mammals: challenges and opportunities. Reprod Fertil Dev 35:118–124

Chen Q, Yan M, Cao Z, Li X, Zhang Y, Shi J, Feng GH, Peng H, Zhang X, Zhang Y et al (2016a) Sperm tsRNAs contribute to intergenerational inheritance of an acquired metabolic disorder. Science 351:397–400

Chen Q, Yan W, Duan E (2016b) Epigenetic inheritance of acquired traits through sperm RNAs and sperm RNA modifications. Nat Rev Genet 17:733–743

Chen Q, Zhang X, Shi J, Yan M, Zhou T (2021) Origins and evolving functionalities of tRNA-derived small RNAs. Trends Biochem Sci 46:790–804

Chen Q, Zhou T (2023) Emerging functional principles of tRNA-derived small RNAs and other regulatory small RNAs. J Biol Chem 299:105225

Conine CC, Rando OJ (2022) Soma-to-germline RNA communication. Nat Rev Genet 23:73–88

Cui L, Nie X, Guo Y, Ren P, Guo Y, Wang X, Li R, Hotaling JM, Cairns BR, Guo J (2025) Single-cell transcriptomic atlas of the human testis across the reproductive lifespan. Nat Aging 5:658–674

Ding Y, Zuo Y, Zhang B, Fan Y, Xu G, Cheng Z, Ma S, Fang S, Tian A, Gao D et al (2025) Comprehensive human proteome profiles across a 50-year lifespan reveal aging trajectories and signatures. Cell 188:5763–5784.e26

Donkin I, Versteyhe S, Ingerslev LR, Qian K, Mechta M, Nordkap L, Mortensen B, Appel EV, Jorgensen N, Kristiansen VB et al (2016) Obesity and bariatric surgery drive epigenetic variation of spermatozoa in humans. Cell Metab 23:369–378

Gapp K, Jawaid A, Sarkies P, Bohacek J, Pelczar P, Prados J, Farinelli L, Miska E, Mansuy IM (2014) Implication of sperm RNAs in transgenerational inheritance of the effects of early trauma in mice. Nat Neurosci 17:667–669

Guo Y, Bai D, Liu W, Liu Y, Zhang Y, Kou X, Chen J, Wang H, Teng X, Zuo J et al (2021) Altered sperm tsRNAs in aged male contribute to anxiety-like behavior in offspring. Aging Cell 20:e13466

Guzzi N, Ciesla M, Ngoc PCT, Lang S, Arora S, Dimitriou M, Pimkova K, Sommarin MNE, Munita R, Lubas M et al (2018) Pseudouridylation of tRNA-derived fragments steers translational control in stem cells. Cell 173:1204–1216 e1226

Hua M, Liu W, Chen Y, Zhang F, Xu B, Liu S, Chen G, Shi H, Wu L (2019) Identification of small non-coding RNAs as sperm quality biomarkers for in vitro fertilization. Cell Discov 5:20

Isacson S, Karlsson K, Zalavary S, Asratian A, Kugelberg U, Liffner S, Ost A (2025) Small RNA in sperm-paternal contributions to human embryo development. Nat Commun 16:6571

Jenkins TG, Aston KI, Pflueger C, Cairns BR, Carrell DT (2014) Age-associated sperm DNA methylation alterations: possible implications in offspring disease susceptibility. PLoS Genet 10:e1004458

Jimbo M, Kunisaki J, Ghaed M, Yu V, Flores HA, Hotaling JM (2022) Fertility in the aging male: a systematic review. Fertil Steril 118:1022–1034

Khandwala YS, Baker VL, Shaw GM, Stevenson DK, Lu Y, Eisenberg ML (2018) Association of paternal age with perinatal outcomes between 2007 and 2016 in the United States: population based cohort study. BMJ 363:k4372

Khandwala YS, Zhang CA, Lu Y, Eisenberg ML (2017) The age of fathers in the USA is rising: an analysis of 168 867 480 births from 1972 to 2015. Hum Reprod 32:2110–2116

Kuhle B, Chen Q, Schimmel P (2023) tRNA renovatio: rebirth through fragmentation. Mol Cell 83:3953–3971

Kunisaki J, Goldberg ME, Lulla S, Sasani T, Hiatt L, Nicholas TJ, Liu L, Torres-Arce E, Guo Y, James E, Horns JJ, Ramsay JM, Chen Q, Hotaling JM, Aston KI, Quinlan AR (2024) Sperm from infertile, oligozoospermic men have elevated mutation rates. Preprint at *medRxiv* https://doi.org/10.1101/2024.08.22.24312232

Liang G, Zhu X, Zhang Z, Chen L, Feng H, Zhan S, Hu H, Yu R, Zhang CY, Feng Z et al (2022) microRNAs in aged sperm confer psychiatric symptoms to offspring through causing the dysfunction of estradiol signaling in early embryos. Cell Discov 8:63

Liu J, Shi J, Hernandez R, Li X, Konchadi P, Miyake Y, Chen Q, Zhou T, Zhou C (2023) Paternal phthalate exposure-elicited offspring metabolic disorders are associated with altered sperm small RNAs in mice. Environ Int 172:107769

Lucas MC, Pryszcz LP, Medina R, Milenkovic I, Camacho N, Marchand V, Motorin Y, Ribas de Pouplana L, Novoa EM (2023) Quantitative analysis of tRNA abundance and modifications by nanopore RNA sequencing. Nat Biotechnol 42:72–86

Mao Y, Zhao Y, Luo S, Chen H, Liu X, Wu T, Ding G, Liu X, Sheng J, Meng Y et al (2022) Advanced paternal age increased metabolic risks in mice offspring. Biochim Biophys Acta Mol Basis Dis 1868:166355

Miyahara K, Tatehana M, Kikkawa T, Osumi N (2023) Investigating the impact of paternal aging on murine sperm miRNA profiles and their potential link to autism spectrum disorder. Sci Rep 13:20608

Natt D, Kugelberg U, Casas E, Nedstrand E, Zalavary S, Henriksson P, Nijm C, Jaderquist J, Sandborg J, Flinke E et al (2019) Human sperm displays rapid responses to diet. PLoS Biol 17:e3000559

Neville MDC, Lawson ARJ, Sanghvi R, Abascal F, Pham MH, Cagan A, Nicola PA, Bayzetinova T, Baez-Ortega A, Roberts K et al (2025) Sperm sequencing reveals extensive positive selection in the male germline. Nature 647:421–428

Nie, Munyoki X, Sukhwani SK, Schmid M, Missel N, Emery A, DonorConnect BR, Stukenborg JB, Mayerhofer A, Orwig KE et al (2022) Single-cell analysis of human testis aging and correlation with elevated body mass index. Dev Cell 57:1160–1176 e1165

Peng H, Shi J, Zhang Y, Zhang H, Liao S, Li W, Lei L, Han C, Ning L, Cao Y et al (2012) A novel class of tRNA-derived small RNAs extremely enriched in mature mouse sperm. Cell Res 22:1609–1612

Ramesh R, Skog S, Orkenby L, Kugelberg U, Natt D, Ost A (2023) Dietary sugar shifts mitochondrial metabolism and small RNA biogenesis in sperm. Antioxid Redox Signal 38:1167–1183

Robinson MD, McCarthy DJ, Smyth GK (2010) edgeR: a Bioconductor package for differential expression analysis of digital gene expression data. Bioinformatics 26:139–140

Sarker G, Sun W, Rosenkranz D, Pelczar P, Opitz L, Efthymiou V, Wolfrum C, Peleg-Raibstein D (2019) Maternal overnutrition programs hedonic and metabolic phenotypes across generations through sperm tsRNAs. Proc Natl Acad Sci USA 116:10547–10556

Seplyarskiy V, Moldovan MA, Koch E, Kar P, Neville MDC, Rahbari R, Sunyaev S (2025) Hotspots of human mutation point to clonal expansions in spermatogonia. Nature 647:429–435

Sharma U, Conine CC, Shea JM, Boskovic A, Derr AG, Bing XY, Belleannee C, Kucukural A, Serra RW, Sun F et al (2016) Biogenesis and function of tRNA fragments during sperm maturation and fertilization in mammals. Science 351:391–396

Shen X, Wang C, Zhou X, Zhou W, Hornburg D, Wu S, Snyder MP (2024) Nonlinear dynamics of multi-omics profiles during human aging. Nat Aging 4:1619–1634

Sherman BT, Hao M, Qiu J, Jiao X, Baseler MW, Lane HC, Imamichi T, Chang W (2022) DAVID: a web server for functional enrichment analysis and functional annotation of gene lists (2021 update). Nucleic Acids Res 50:W216–W221

Shi J, Chen Q, Li X, Zheng X, Zhang Y, Qiao J, Tang F, Tao Y, Zhou Q, Duan E (2015) Dynamic transcriptional symmetry-breaking in pre-implantation mammalian embryo development revealed by single-cell RNA-seq. Development 142:3468–3477

Shi J, Ko EA, Sanders KM, Chen Q, Zhou T (2018) SPORTS1.0: a tool for annotating and profiling non-coding RNAs optimized for rRNA- and tRNA-derived small RNAs. Genomics Proteomics Bioinformatics 16:144–151

Shi J, Zhang Y, Li Y, Zhang L, Zhang X, Yan M, Chen Q, Zhang Y (2025) Optimized identification and characterization of small RNAs with PANDORA-seq. Nat Protoc 20:3314–3338

Shi J, Zhang Y, Tan D, Zhang X, Yan M, Zhang Y, Franklin R, Shahbazi M, Mackinlay K, Liu S et al (2021) PANDORA-seq expands the repertoire of regulatory small RNAs by overcoming RNA modifications. Nat Cell Biol 23:424–436

Shi J, Zhou T, Chen Q (2022) Exploring the expanding universe of small RNAs. Nat Cell Biol 24:415–423

Su Z, Monshaugen I, Wilson B, Wang F, Klungland A, Ougland R, Dutta A (2022) TRMT6/61A-dependent base methylation of tRNA-derived fragments regulates gene-silencing activity and the unfolded protein response in bladder cancer. Nat Commun 13:2165

Taylor JL, Debost JPG, Morton SU, Wigdor EM, Heyne HO, Lal D, Howrigan DP, Bloemendal A, Larsen JT, Kosmicki JA et al (2019) Paternal-age-related de novo mutations and risk for five disorders. Nat Commun 10:3043

Thompson DM, Lu C, Green PJ, Parker R (2008) tRNA cleavage is a conserved response to oxidative stress in eukaryotes. RNA 14:2095–2103

Tomar A, Gomez-Velazquez M, Gerlini R, Comas-Armangue G, Makharadze L, Kolbe T, Boersma A, Dahlhoff M, Burgstaller JP, Lassi M et al (2024) Epigenetic inheritance of diet-induced and sperm-borne mitochondrial RNAs. Nature 630:720–727

Watson C (2025) The search for mutations that sperm acquire as men age. Nature 647:323–324

Yuan X, Su Y, Johnson B, Kirchner M, Zhang X, Xu S, Jiang S, Wu J, Shi S, Russo JJ et al (2024) Mass spectrometry-based direct sequencing of tRNAs de novo and quantitative mapping of multiple RNA modifications. J Am Chem Soc 146:25600–25613

Zhang Y, Ren L, Sun X, Zhang Z, Liu J, Xin Y, Yu J, Jia Y, Sheng J, Hu GF et al (2021) Angiogenin mediates paternal inflammation-induced metabolic disorders in offspring through sperm tsRNAs. Nat Commun 12:6673

Zhang Y, Shi J, Rassoulzadegan M, Tuorto F, Chen Q (2019) Sperm RNA code programmes the metabolic health of offspring. Nat Rev Endocrinol 15:489–498

Zhang Y, Zhang X, Shi J, Tuorto F, Li X, Liu Y, Liebers R, Zhang L, Qu Y, Qian J et al (2018) Dnmt2 mediates intergenerational transmission of paternally acquired metabolic disorders through sperm small non-coding RNAs. Nat Cell Biol 20:535–540

Acknowledgements

This work is in part supported by NIH (R01HD092431 to QC, TZ, MP, and DM; R01ES032024 to QC and TZ; R35ES035015 to CZ, QC, and TZ; R01HD106112 to KI, JH, and AQ; R00HD111686 to XY), research funds from Induction Bio. (to QC and TZ), University of Utah startup funds (to QC) and Center for Genomic Medicine Pilot Award from University of Utah (to QC). This work includes data generated at the University of California, San Diego IGM Genomics Center funded by the NIH (P30DK063491, P30CA023100, and P30DK120515).

Author contributions

Junchao Shi: Conceptualization; Formal analysis; Investigation; Methodology; Writing—original draft; Writing—review and editing. **Xudong Zhang**: Conceptualization; Data curation; Investigation; Writing—original draft; Writing—review and editing. **Chen Cai**: Data curation; Investigation; Writing—review and editing. **Shichao Liu**: Investigation. **Jiancheng Yu**: Data curation; Writing—review and editing. **Emma R James**: Resources; Investigation. **Lihua Liu**: Resources. **Benjamin R Emery**: Resources. **Megan R McMurray Bires**: Formal analysis. **Elizabeth Torres-Arce**: Investigation. **Hukam C Rawal**: Methodology; Writing—review and editing. **Joemy Ramsay**: Data curation. **Jason Kunisaki**: Data curation. **Changcheng Zhou**: Funding acquisition; Writing—review and editing. **David S Milstone**: Funding acquisition; Writing—review and editing. **Mary Elizabeth Patti**: Funding acquisition; Writing—review and editing. **Xiaoxu Yang**: Formal analysis; Writing—review and editing. **Tim G Jenkins**: Formal analysis; Writing—review and editing. **Aaron Quinlan**: Formal analysis; Funding acquisition; Writing—review and editing. **Bradley R Cairns**: Formal analysis; Writing—review and editing. **Paul Schimmel**: Formal analysis; Writing—review and editing. **James M Hotaling**: Resources; Funding acquisition; Writing—review and editing. **Kenneth I Aston**: Resources; Supervision; Funding acquisition; Writing—review and editing. **Tong Zhou**: Conceptualization; Formal analysis; Supervision; Funding acquisition; Methodology; Writing—original draft; Writing—review and editing. **Qi Chen**: Conceptualization; Formal analysis; Supervision; Funding acquisition; Writing—original draft; Writing—review and editing.

Source data underlying figure panels in this paper may have individual authorship assigned. Where available, figure panel/source data authorship is listed in the following database record: biostudies:S-SCDT-10_1038-S44318-025-00687-8.

Disclosure and competing interests statement

JH is a clinical advisor for Induction Bio. The remaining authors declare no competing interests.

Expanded View Figures

Figure EV1. miRNA "aging cliff".

miRNA profiles detected by PANDORA-seq show an aging cliff in intact sperm (**A–D**) and sperm heads (**E–H**) during mouse aging but is less prominent than the tsRNA/rsRNA profiles. (**A**) Illustrative figure showing the intact sperm collection at five time points (10-, 30-, 50-, 70-, and 90-week) during mouse aging. (**B**, **C**) Principal coordinate analysis (PCoA) of mouse sperm miRNA profiles showing that (**B**) PANDORA-seq, but not (**C**) traditional sncRNA-seq, identified an "aging cliff" during the 50–70-week transition in mouse sperm. Axis 1: the first principal coordinate; Axis 2: the second principal coordinate. (**D**) The ratio of between-group variance to within-group variance (*F*-statistic) is significantly higher in tsRNA/rsRNA group than that of the miRNA group in PANDORA-seq data, supporting that tsRNA/rsRNA profile shows a better classification power than miRNA profile between the demarcated stages (early 10-/30-/50-week vs. later 70-/90-week). The *P* value was computed by Wilcoxon test. (**E–H**) similar analyses on purified sperm heads as those of (**A–D**). For boxplot in (**D**, **H**), the bold horizontal line indicates the median of the data. The lower and upper box boundaries of the box indicate the 25th percentile (Q1) and 75th percentile (Q3) of the data, respectively. Accordingly, the interquartile range (IQR) is Q3-Q1. The lower and upper whiskers indicates the most extreme data points that fall within Q1-1.5 × IQR and Q3 + 1.5 × IQR, respectively. For (**D**): $n = 1005$ for miRNA and $n = 81$ for tsRNA/rsRNA; For (**H**): $n = 950$ for miRNA and $n = 81$ for tsRNA/rsRNA.

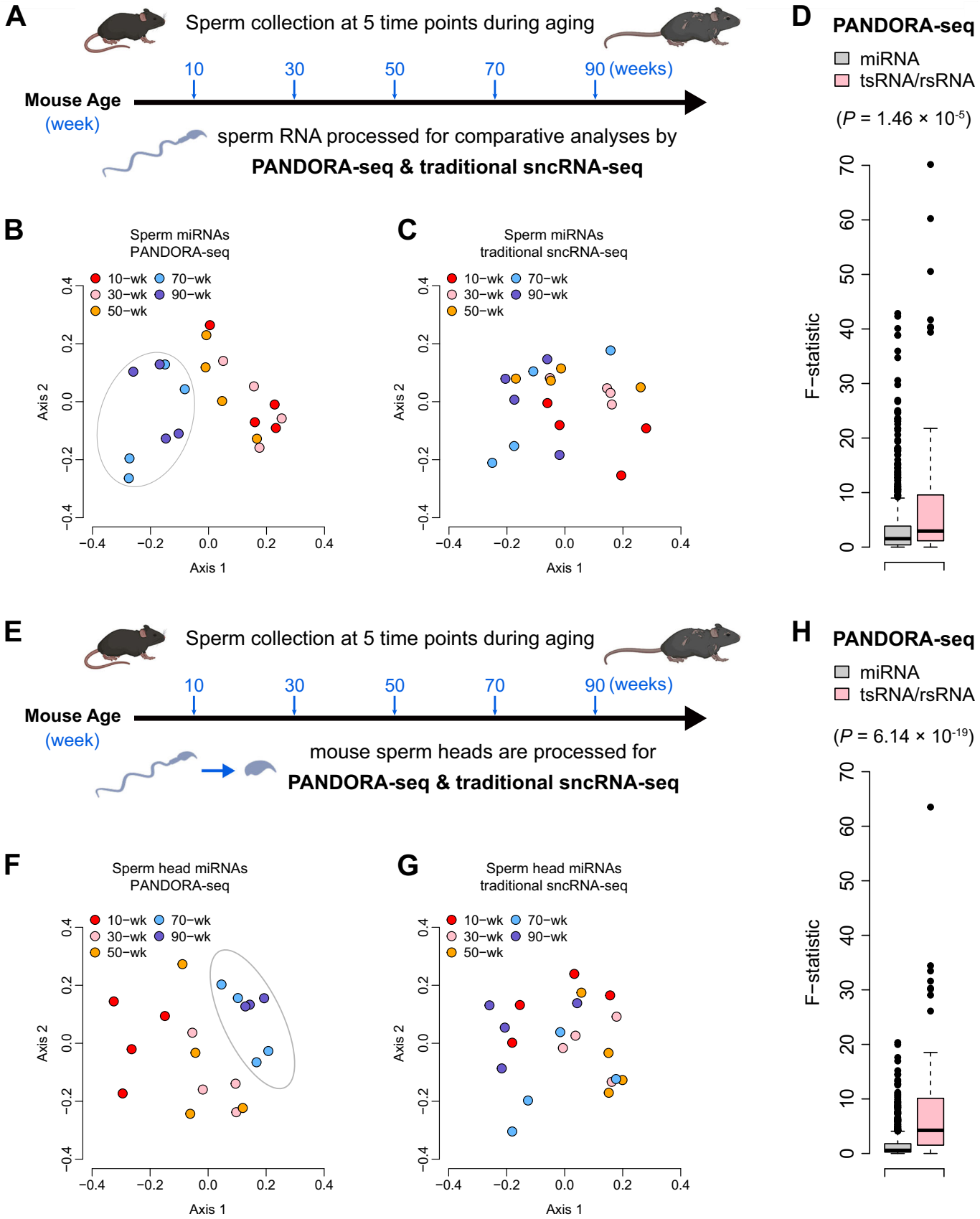
A
Sperm collection at 5 time points during aging
10
30
50
70
90 (weeks)
Mouse Age
(week)
sperm RNA processed for comparative analyses by
PANDORA-seq & traditional sncRNA-seq
B
Sperm miRNAs
PANDORA-seq
C
Sperm miRNAs
traditional sncRNA-seq
10−wk
70−wk
30−wk
90−wk
50−wk
Axis 1
Axis 2
D
PANDORA-seq
miRNA
tsRNA/rsRNA
(P = 1.46 × 10-5)
F−statistic
E
Sperm collection at 5 time points during aging
Mouse Age
(week)
mouse sperm heads are processed for
PANDORA-seq & traditional sncRNA-seq
F
Sperm head miRNAs
PANDORA-seq
G
Sperm head miRNAs
traditional sncRNA-seq
H
PANDORA-seq
miRNA
tsRNA/rsRNA
(P = 6.14 × 10-19)
F−statistic

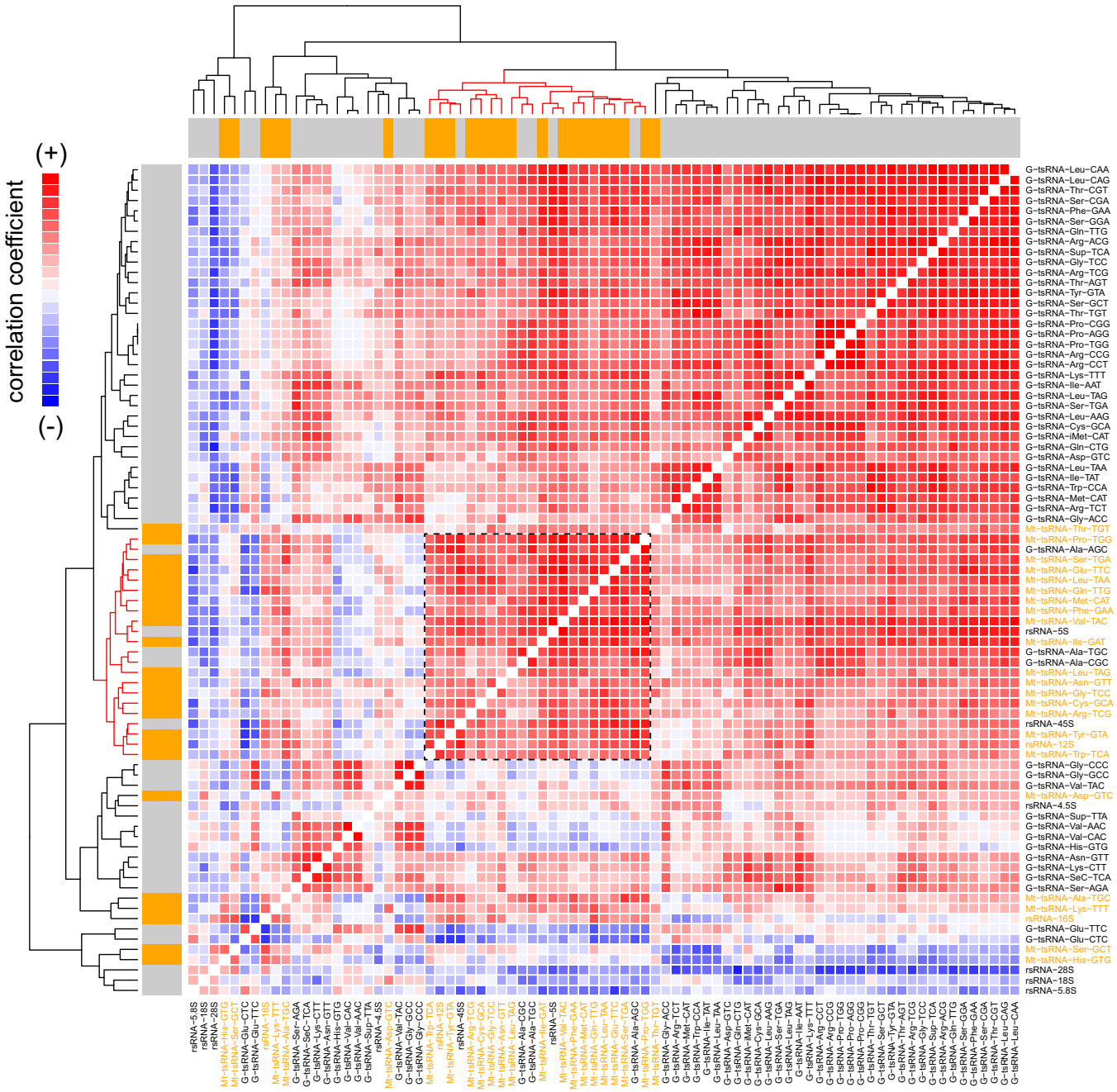

Figure EV2. Co-expression pattern of all the genomic tsRNAs/rsRNAs and mitochondrial tsRNAs/rsRNAs in the mouse de-membranated sperm heads.

The colors in the heatmap represent the intensity of co-expression (i.e., Spearman's rank correlation coefficient) between the sncRNAs: red indicates positive co-expression, while blue indicates negative co-expression. This co-expression pattern is a magnified version of Fig. 1G, showing the identity of each tsRNA/rsRNA category on the heatmap. The enriched mt-tsRNA/rsRNA cluster (the dashed area in the middle) suggests that these mitochondrial sncRNAs are transcribed or regulated in a coordinated manner, which may reflect that, in the mature sperm, the genomic transcription is silent while the mitochondrial DNA transcription remains active. G-tsRNA genomic tsRNA, Mt-tsRNA mitochondrial tsRNA.

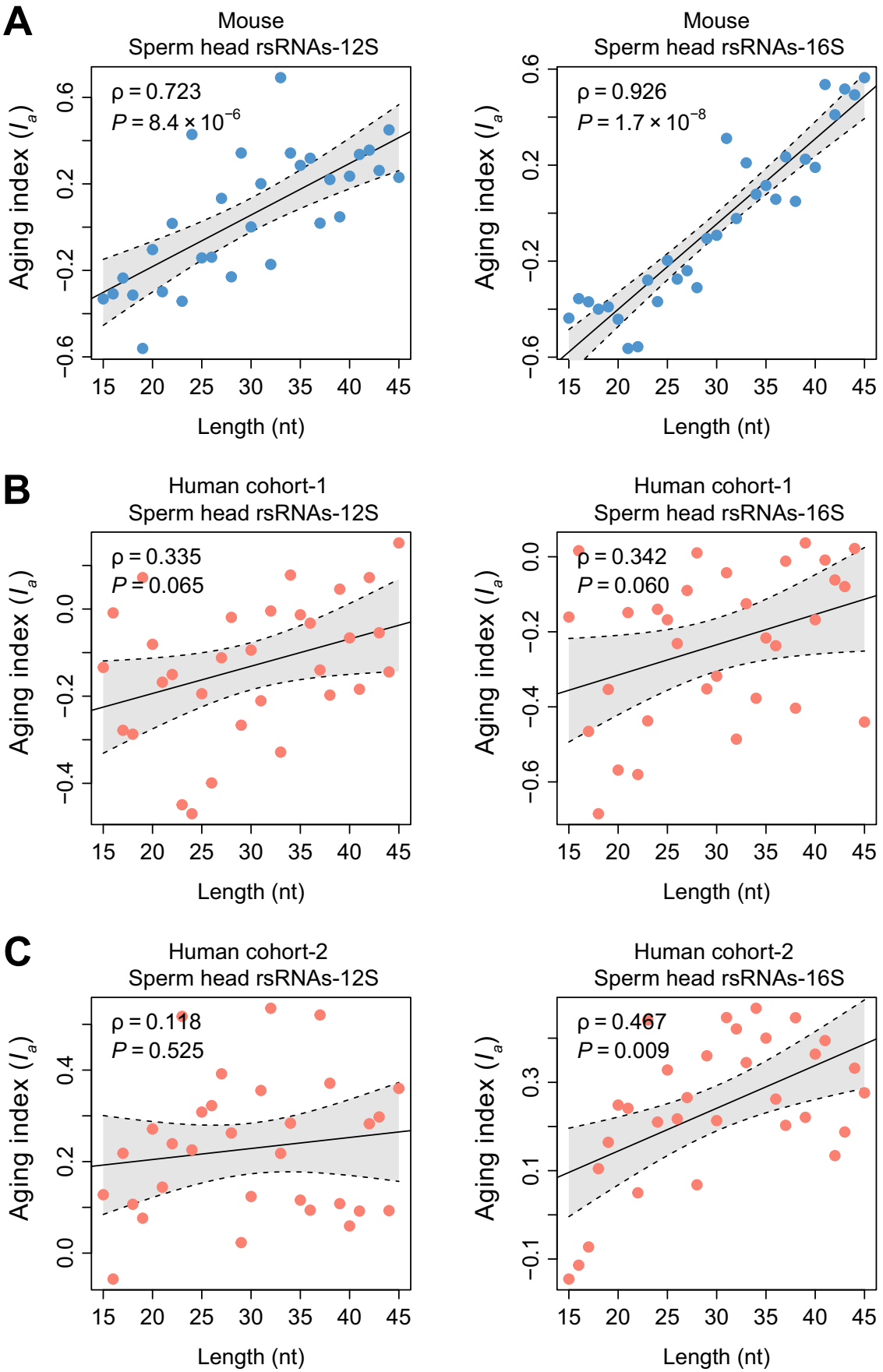
A
Mouse
Sperm head rsRNAs-12S
ρ = 0.723
P = 8.4 × 10−6
Aging index (Ia)
Length (nt)
Mouse
Sperm head rsRNAs-16S
ρ = 0.926
P = 1.7 × 10−8
B
Human cohort-1
Sperm head rsRNAs-12S
ρ = 0.335
P = 0.065
Human cohort-1
Sperm head rsRNAs-16S
ρ = 0.342
P = 0.060
C
Human cohort-2
Sperm head rsRNAs-12S
ρ = 0.118
P = 0.525
Human cohort-2
Sperm head rsRNAs-16S
ρ = 0.467
P = 0.009

Figure EV3. Age-related length shift of mitochondrial rsRNAs (12S, 16S) in mouse and human sperm heads.

RNA sample was extracted from de-membranated sperm heads from (**A**) mouse during 10–90 weeks as that of Fig. 2A, (**B**) human cohort-1, and (**C**) human cohort-2 as that of Fig. 3A, B, followed by PANDORA-seq. We calculated the association of expression (RPM) with age (Spearman's correlation), which we termed as aging index (I_a). Each dot represents the value of I_a for the corresponding length. The scatter plots demonstrate the relationship between I_a and RNA length, which was measured by Spearman's rank correlation coefficient (ρ) and the corresponding P value. The solid lines depict linear regression fits.

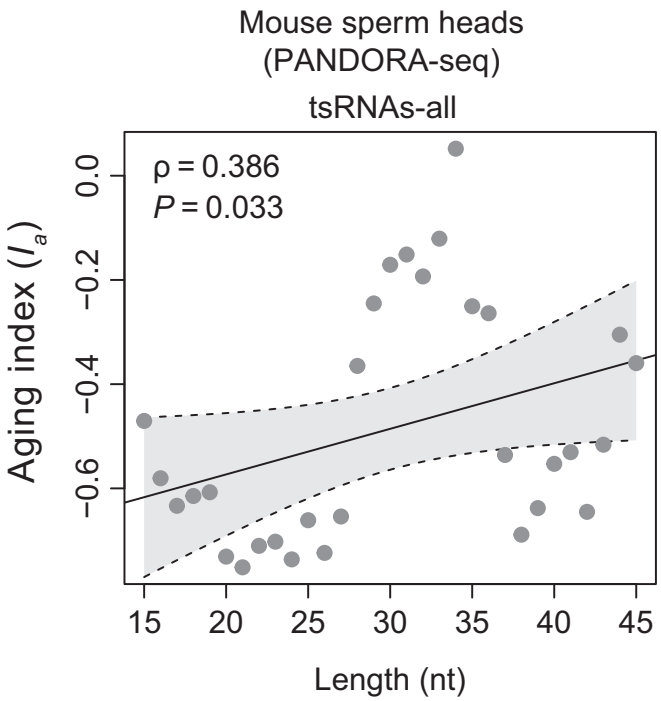

Figure EV4. Less prominent age-related length shift of tsRNAs in mouse sperm heads.

Age-related length shift analyses of tsRNAs are similarly performed as that of rsRNAs in Fig. 2A, where sncRNAs were extracted from de-membranated sperm heads followed by PANDORA-seq. We calculated the association of expression (RPM) with age (Spearman's rank correlation), which we termed as aging index (I_a). Each dot represents the value of I_a for the corresponding length. The scatter plots demonstrate the relationship between I_a and RNA length, which was measured by Spearman's rank correlation coefficient (ρ) and the corresponding *P* value. The solid lines depict linear regression fits. The figure shows that the age-related length shift in tsRNAs is less prominent compared to that of rsRNAs in sperm heads.